

CHARACTERIZATION OF STRAIN RATE DEPENDENCE IN THE MECHANICAL BEHAVIOR OF GOLD THIN FILMS

Colin P. Bateson
Mechanical and Aerospace Engineering
University of Virginia
Charlottesville, Virginia 22904
E-mail: bateson@virginia.edu

Advisor: Dr. Ioannis Chasiotis
Aerospace Engineering
University of Illinois at Urbana-Champaign
Urbana, Illinois 61801
E-mail: chasioti@uiuc.edu

ABSTRACT

The effect of strain rate on the mechanical behavior of gold thin-films for RF-MEMS applications was examined. Microscale, free-standing, dog bone shaped specimens were subjected to uniaxial tension tests at strain rates ranging between 10^{-6} s^{-1} and 10^{-3} s^{-1} via a custom built testing apparatus. The specimens, fabricated using e-beam evaporation, had gage sections 1000 μm long and 200 μm wide, with thickness varying between 500 and 650 nm. The specimens were fabricated as 200 nm multi-layers with 100 nm average grain size. Force and displacement data were collected and used to construct stress-strain curves. The specimens exhibited elastic-nearly perfectly plastic behavior at all strain rates excluding the slowest (10^{-6} s^{-1}) where local stress peaks were observed. Material yield strength and peak stress, ranging from 120-300 MPa and 140-365 MPa respectively, both increased as the strain rate increased. For high strain rates the ductility was measured to be about 1.9%, increasing to 4.5% for the lowest strain rate. These values were found to be consistent with those published in literature. In general, the material exhibited qualitative trends as expected for the variation in strain rate except, as mentioned before, at the slowest strain rates.

INTRODUCTION

Microelectromechanical Systems (MEMS) have the potential to revolutionize the space industry. Some of the space specific advantages of MEMS include the drastic reduction in mass, volume, and power requirements. This will directly impact spacecraft, test facilities, and most important, launch costs.^[1] However, the utilization of MEMS in space applications has been limited due to concerns about their reliability and survivability in the harsh space environment.^[2] Only thorough testing of MEMS devices and materials will ever abate these concerns.

Gold has been identified as an ideal candidate material for radio frequency (RF) MEMS due to its chemical inertness, low processing temperature, and outstanding electrical conductivity. A literature survey showed that testing of gold thin films is a recent development and much about the mechanical behavior at the microscale is still uncertain. Gudlavalletti *et al.* studied the stress-strain response of gold thin films as early as 2002, reporting values for ductility, yield and maximum stress.^[3] Espinosa and Prorok have done

studies on gold thin films since 2003 investigating size-effects on mechanical behavior using a Membrane Deflection Experiment (MDE).^[4] More recently in 2003, Li and Cima conducted bulge tests on gold thin films reporting values for bulk modulus and yield strength, the later of which were slightly higher than those values measured by Espinosa and Prorok.^[5] This research project was designed to investigate the effects of strain rate on the mechanical behavior of gold thin films focusing specifically on the changes in ductility, yield stress, and strength as a function of strain rate.

MATERIALS

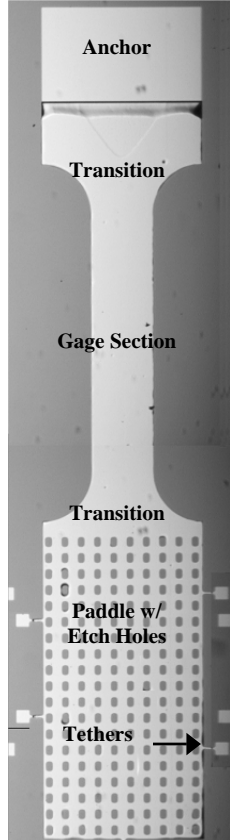
Specimen Fabrication

The specimens used for this research project were freestanding evaporated gold thin films fabricated in Univ. of Virginia's Microfabrication Laboratory using modern photolithographic techniques. First, a silicon wafer was covered with AZ4110 photoresist and spun up to 7000 RPM for 30 seconds. This resulted in a layer of photoresist 0.7 μm thick. The wafer was then allowed to sit for a few minutes before it was softbaked

to solidify the photoresist. Next, the anchor holes were patterned and etched out of the photoresist. This allowed the bimetallic layer of titanium (Ti) and gold (Au) evaporated onto the wafer to adhere to the silicon and form the anchor points, while the rest of the metallic layer was evaporated up on top of the photoresist. The layer of Ti is used to help the Au stick to the silicon wafer, something Au does not do well on its own. After the initial 100 Å layer of Ti, subsequent layers of gold 2000 Å thick were deposited until the total desired specimen thickness was reached. This was done to insure that the microstructure and grain size of the specimens remained constant regardless of specimen thickness. After the evaporation process, the specimen outline and paddle etch holes were then patterned and etched out of the gold. The removal of the remaining photoresist resulted in a set of freestanding specimens. The wafer with freestanding specimens was submersed in hydrofluoric (HF) acid to remove the Ti layer, and then finally the specimens were released using a CO₂ critical point dryer.

Specimen Geometry

The specimens were fabricated into a classic tensile test dog bone shape. Their geometry is most easily described by dividing the specimens into specific sections. These sections have been labeled in Figure 1.



The anchor section is evaporated directly onto the silicon substrate, and as the name suggests, serves as the anchoring point for the test specimen. On the other side of the specimen is the paddle. This is where the specimen is gripped and pulled. The gage section in the middle of the specimen is the most critical component because this is the region where failure occurs and ideally it should be free of defects or flaws. The long length and uniform width, combined with the smooth circular transition sections, are designed to ensure a uniform stress distribution throughout the gage section. As mentioned previously, the gage and paddle sections are fabricated on top of a sacrificial layer of photoresist that is removed in one of the

Figure 1: Evaporated gold specimen with sections labeled

final stages of fabrication leaving the specimens suspended in midair, hence the term freestanding. To protect the specimens prior to testing, the paddle is secured to the silicon wafer with tethers connected to anchor tabs that are firmly attached to the silicon substrate just like the anchor. The paddle is filled with etch holes to facilitate the removal of photoresist by increasing the surface area exposed to the etchant, and to facilitate glue adhesion between the test grip and the specimen.

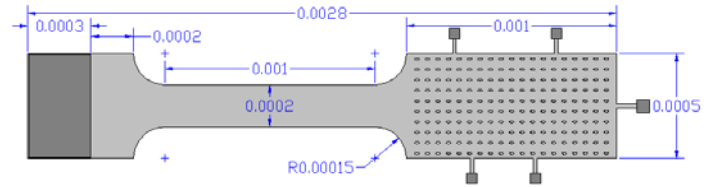


Figure 2: Evaporated gold specimen with dimensions in meters

The gage section of the specimens is 1000 μm long and 200 μm wide. Including the anchor and the paddle, a specimen measures 2800 μm long overall. The original intent was to manufacture specimens with three different thicknesses (200nm, 600nm, 800nm) to add an additional test variable to the experiments, but due to some fabrication difficulties with residual stresses in the material, the manufacturing process had to be optimized to minimize these stresses. As a result, the variation in thickness was much smaller than anticipated (650nm, 530nm, 500nm).

Equipment

As mentioned before, the specimens were manufactured with anchor tabs and tethers to protect the freestanding portion of the specimen. This meant that prior to testing these tethers needed to be broken. This task was performed using a device termed a probing station. This probing station consisted of a small chuck mounted on four translation stages – one stage for each of the three directions and then a fourth that moved in line with the chuck. A very fine pointed wire was held in the chuck, and the translation stages were manipulated to move the wire and prepare the specimen for testing.

The custom built tensile tester consisted of a piezoelectric linear actuator and a low force load cell. Both the actuator and the load cell were mounted on translation stages the combination of which allowed for movement in all three directions as well as rotation about the axis of travel of the actuator. The translation stages were used to accurately align the specimen with the actuator and the load cell to ensure a truly uniaxial tensile test. The actuator came with an independent controller, which was in turn controlled through a computer. The load cell output was connected to a

digital multimeter (DMM) that was attached to the same computer.

METHODOLOGY

Specimen Preparation

The specimens were received from the fabrication lab in the form of one silicon wafer diced into four 1x1 cm squares of 20 specimens each. Two of these four chips had specimens with uniform gage sections of the type used in this experiment – ten specimens on each of these two chips for a total of 20 uniform specimens. One of these silicon squares was then glued to a small aluminum square with super glue. The purpose of the aluminum square was to provide a surface to handle and secure in the test setup. The aluminum block with the specimens was then examined under a microscope and detailed notes were made on the quality and appearance of the specimens. The best-looking specimens were identified and marked for testing. Digital images were taken of all the specimens prior to testing to allow for comparison to similar images taken after testing. Next, the specimens were secured for probing.

The probing station, as described previously in chapter two, was used to prepare the specimens for testing. First, the anchor tethers had to be broken to free a single specimen. After the tethers were broken, the aluminum block was turned 90 degrees, and the wire was worked all the way underneath the specimen to make sure that it was raised up off the silicon substrate and truly freestanding. At this point, the specimen was ready to mount in the test setup.

Test Setup and Preparation

The first step of preparation for testing involved cutting very thin strips of glass out of microscope slide covers. These “glass grips,” as they were called, were directly attached to the paddle section of the specimen, and it was through this grip that a displacement was imposed on the specimen. The grips had to be examined under a microscope to verify that the tip was extremely square. This was important to avoid creating asymmetric stress distributions or stress concentrations in the specimen that would lead to undesirable premature failure. Once an acceptable grip was decided upon, it was attached to a specially fabricated “glass grip holder” that served as an interface between the actuator and the glass grip. The grip was secured with an ultraviolet-curable (UV) adhesive, and special care was taken to make sure that cure times were consistent for all the experiments. Next, the aluminum block with the probed specimen was mounted onto the load cell, and after securing the glass grip and grip holder onto the actuator, the entire test

setup was meticulously aligned. At this point, the actuator was then removed from its translation stage and UV adhesive was applied to the tip of the glass grip. The actuator was then remounted and the specimen was slowly moved up to meet the grip using a translation stage attached to the load cell. After inspecting the connection between the specimen paddle and the glass grip for alignment, positioning, and glue coverage, the adhesive was exposed to UV light and permanently cured.

Running the Test

After the UV light source was removed, the specimen was very slightly buckled to remove any stress put on the specimen in the mounting process. This also ensured that the entirety of the stress strain response would be captured. At this point, the two data collection computer programs were configured and prepared for testing. The next step required waiting patiently for the temperature of the room and the specimen to stabilize. The setup was considered stable when the load cell voltage fluctuated less than 1% of the maximum voltage expected for the experiment over a time period equal to the duration of the experiment. When a stable condition was reached, the computer programs were started and the test commenced.

Data Collection

The computer programs collected the load cell voltage values corresponding to the load on the test setup, and the actuator voltage values corresponding to the location of the actuator, or more important, the displacement imposed on the specimen. Computer time stamp values were attached to both voltage readings to allow for the independent data files to be matched together. This data was then stored in text files that were later manipulated in MATLAB resulting in load and displacement data arrays. These arrays were then plugged into Excel worksheets created to process the data and graphically portray the results.

Calibration Tests

In order to quantify the accuracy of the data collected, calibration experiments were conducted to test various parts of the experimental setup. First, the data collection capabilities of the computer and concomitant hardware needed to be assessed. This was done by connecting a function generator and an oscilloscope to the digital multimeter (DMM) and sampling various functions at increasing frequencies. From these tests it was concluded that accuracy dropped significantly when the computer was asked to sample at a rate slightly higher than 20Hz. As a result,

all subsequent tests, including those included in this paper, were conducted at a data-sampling rate of 20 Hz.

The second calibration test consisted of quantifying the compliance of the load cell and the rest of the test setup. The load cell however was significantly more compliant than any of the other components. Therefore this compliance factor is referred to as the load cell compliance in the data processing worksheets. Since the data collected from the actuator represented to total displacement of the entire test setup, it was necessary to know the compliance of setup without a test specimen so that this displacement could be subtracted from the raw data. This test was performed by setting up for a normal tensile test, but instead of curing the glass grip to a test specimen, the grip was cured directly to the silicon substrate. This resulted in a calibration factor for the displacement of the test setup minus the test specimen as a function of load cell voltage. It should be noted that the load cell compliance was accountable for approximately 10% of the total measured displacement at the maximum load observed throughout the entirety of the experiments.

The third and final calibration test was performed to assess the rate sensitivity of the test setup. For this calibration, tensile tests were conducted with amorphous brittle specimens with a known elastic modulus and similar dimensions to those of the Au specimens. The test results were very repeatable regardless of strain rate therefore showing that the testing setup had negligible rate sensitivity.

Data Processing

The data collection programs would output two text files, one for the load cell and one for the actuator. These files were run through a MATLAB

program designed to compare the two text files and then match the corresponding voltage values based on the computer time stamp associated with each data point. The voltage values were then written to new text files and subsequently imported into Excel worksheets created to automatically process the data.

Worksheets for specimens of the same thickness were combined and the stress-strain (σ - ϵ) curves were plotted together on the same graph. These curves were then color coded according to strain rate to help visualize any data trends. To determine the yield point and elastic limits, individual σ - ϵ plots were printed out and the values were measured by hand. All the data was collected and tabulated in a separate Excel file and then sorted by strain rate. Multiply sets of data with the same strain rate and specimen thickness were averaged and then added to the data table.

RESULTS

Quantitative strain rate trends in the mechanical properties of the thin films were not as prominent as they were expected to be. However, qualitative trends did arise, and interesting results were observed at the slowest strain rate.

Strong rate dependency was observed in the yield and maximum strengths, as well as the ductility. In general, yield and maximum strengths decreased with decreasing strain rate while ductility increased, which was to be expected theoretically. The elastic limit was also measured as this property more accurately describes the actual transition from elastic to plastic deformation in the specimen. The numerical results are summarized in Table 1.

Examination of the stress-strain (σ - ϵ) curves showed that the specimens exhibited elastic-nearly perfectly plastic behavior at all strain rates excluding

Table 1: Properties of Au films as a function of strain rate and film thickness

Specimen thickness (μm)/ Strain rate (s^{-1})	Elastic Limit (MPa)	0.2% Yield Strength (MPa)	Maximum Strength (MPa)	Ductility (%)	Number of Specimens Tested
0.5/ 10^{-3}	125	240	300	2.0	3
0.5/ 10^{-4}	90	200	275	2.4	2
0.5/ 10^{-5}	95	210	200	2.4	1
0.5/ 10^{-6}	95	155	175	4.5	2
0.53 μm group					
0.53/ 10^{-3}	220	300	340	1.9	1
0.53/ 10^{-4}	145	255	315	2.5	1
0.53/ 10^{-5}	140	260	315	3.3	2
0.53/ 10^{-6}	95	125	150	4.2	2
0.65 μm group					
0.65/ 10^{-3}	170	300	365	2.2	1
0.65/ 10^{-4}	140	280	335	2.8	1
0.65/ 10^{-5}	120	235	290	2.3	2
0.65/ 10^{-6}	100	180	230	4.7	1

the slowest (10^{-6} s^{-1}) where local stress peaks were observed. However, these stress peaks failed to appear in the thickest specimens (0.65um) at the 10^{-6} s^{-1} strain rate. The peaks were attributed to the proximity of the material's diffusional creep rate to the slowest strain

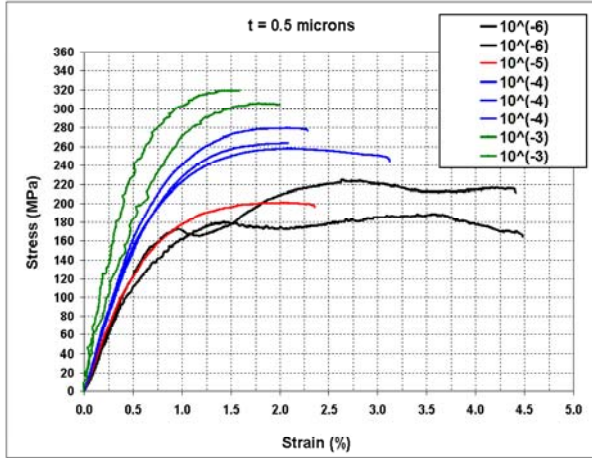


Figure 3: Stress-strain curves for 500nm thick specimens

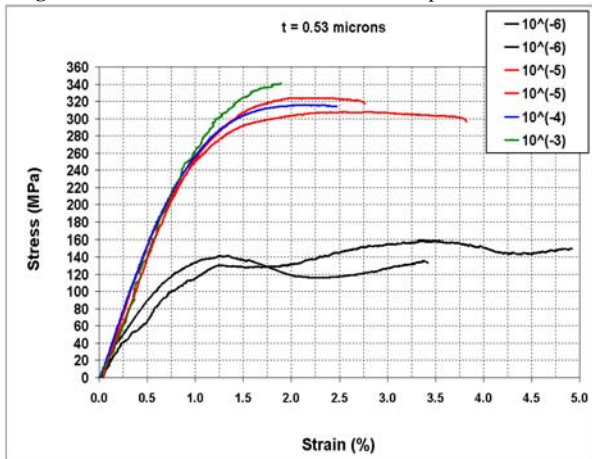


Figure 4: Stress-strain curves for 530nm thick specimens

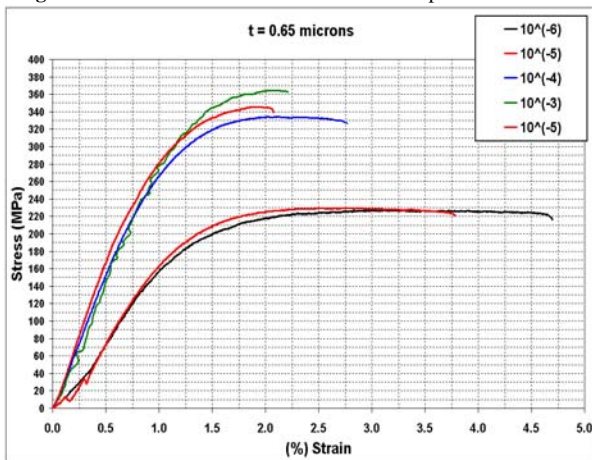


Figure 5: Strain-strain curves for 650nm thick specimens

rate, resulting in a considerable contribution to the total stress-strain behavior from diffusional creep.^[7] The plots included on this page are grouped together by specimen thickness.

The variation in the values for yield strength, maximum strength, and ductility most likely was the result of tiny flaws in the test specimens. Only approximately half of the specimens tested were completely free of visible defects. Defective specimens were avoided whenever possible, but unfortunately necessity forced exceptions to be made. Some of the flaws observed were perfectly linear, extremely faint scratches that sometimes continued across an entire chip of specimens. Other flaws could be described as similar to a small grain of sand squashed between a flat surface and a thin sheet of paper. After each test, the notes made prior to testing. Data from specimens that obviously failed at the same location as a documented flaw was not analyzed.

There were many other potential sources of error inherent in the design of the tensile testing apparatus. First, the specimens had to be aligned by hand in all three directions, which was a difficult task. The specimen gripping and curing processes both had to be done manually. Inconsistencies could have occurred in the placement of the grip on the paddle of the specimen, as well as the amount of glue and time used to cure the grip to the specimens. Lastly, the probing process is not particularly gentle and the elastic limit of the specimens may have been occasionally breached resulting in plastic deformation and strain hardening. Any of these sources of error could have contributed to the uncertainty in the results.

CONCLUSION

The experimental results obtained in this investigation were comparable to those published previously for gold thin films.^[3,4] In general, the stress and ductility trends for rate dependency agreed with predictions made based on current theory. Across a range in strain rates three orders of magnitude ($10^{-3} \text{ s}^{-1} - 10^{-6} \text{ s}^{-1}$) the following was found:

- (1) The 0.2% yield stress varied between 120-300 MPa, and the elastic limit varied between 65-220 MPa, for all thicknesses and strain rates. The lowest stresses correspond to the slowest strain rate, and vice versa.
- (2) The peak stress varied between 140-365 MPa. Again, the lowest stress corresponded to the slowest strain rate, and vice versa.

- (3) The ductility was found to vary between 1.9-4.5%, with the highest ductility corresponding to the slowest strain rate.
- (4) Local peak stresses were observed in the thinnest specimens (530nm, 500nm) at the 10^{-6} s^{-1} strain rate. These peaks were attributed to the proximity of the material's diffusional creep rate to the slowest strain rate, resulting in a considerable contribution to the total stress-strain behavior.
- (5) A strong strain rate dependency was observed in the material ductility, yield stress and peak stress. Ductility was found to decrease with increasing strain rate, while both the yield and peak stresses increased as the strain rate increased.
- [5] Li. 2003. Bulge test on free standing gold thin films. *Materials Research Society Symposium - Proceedings Thin Films - Stresses and Mechanical Properties X* 795: 437-442.
- [6] Harris. 1998. Direct observation of diffusional creep via TEM in polycrystalline thin films of gold. *Acta Materialia* 46, no. 17: 6195-6203.

ACKNOWLEDGMENTS

The author acknowledges the support provided by the Virginia Space Grant Consortium that made this research possible. Additionally, the author thanks the National Science Foundation for their support under REU grant CMS #0301584 as well as the University of Virginia for their generous Harrison Undergraduate Research Award. The author would especially like to thank Katherine Timpano, James Stanec, Amanda McCarty, Charlie Smith, Krishna Jonnalagadda, and Sung Woo Cho for their contributions to this research. Finally, the author expresses his deep appreciation for the time and guidance provided by Dr. Ioannis Chasiotis. Thank you for this tremendous opportunity.

WORKS CITED

- [1] Benoit. 1998. Micro and nanotechnologies: A challenge on the way forward to new markets. *Materials Science*, no. 1-3: 254-257.
- [2] Man. 1999. MEMS reliability for space applications by elimination of potential failure modes through testing and analysis. *Proceedings of SPIE - The International Society for Optical Engineering* 3880: 120-129.
- [3] Gudlavalleti. 2002. Stress-strain response of free-standing nano-crystalline gold thin-films. *Materials Research Society Symposium - Proceedings* 695: 425-430.
- [4] Espinosa. 2003. Size effects on the mechanical behavior of gold thin films. *Journal of Materials Science* 38, no. 20: 4125-4128.